Check for updates

Proceedings of the 2019 Hypervelocity Impact Symposium
HVIS2019
April 14-19, 2019, Destin, FL, USA
HVIS2019-111

Extended Abstract+

Higher-order finite elements for lumped-mass explicit modeling of high-speed impacts

Robert S. Browning[a], Kent T. Danielson[b]*, Ph.D., Mark D. Adley[b], Ph.D., P.E.

[a]Geotechnical & Structures Laboratory, U.S. Army Engineer Research and Development Center
3909 Halls Ferry Road, CEERD-GSM, Vicksburg, MS 39180-6199 USA
[b]Geotechnical & Structures Laboratory, U.S. Army Engineer Research and Development Center
3909 Halls Ferry Road, CEERD-GMR, Vicksburg, MS 39180-6199 USA

1. Introduction and background

Classical finite element analysis (FEA) continues to be a primary computational method of choice for most solid mechanics applications and the explicit method is significantly used in the defense industry for high-speed impact analysis. The explicit lumped-mass approach, without a stiffness matrix, is well suited for rapidly changing/high rate short duration applications, but can produce distinct nuances and severely affect element performances differently than in typical static/implicit methods. In contrast to automatic tetrahedral meshing approaches applied to the entire volume, hexahedral-dominant modeling methods (e.g., [1-3]) attempt to mesh with all hexahedral elements and then automation with other element types is applied only to regions where the Hex mesher has trouble. The methods typically use wedge and/or pyramid elements to transition from hexahedral elements to fill volumes with other types. This results in models that typically have much fewer elements than with "all-Tet" approaches

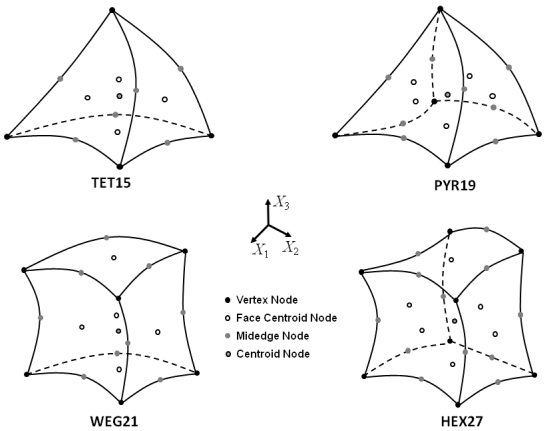

+ Full paper can found at https://www.sciencedirect.com/journal/international-journal-of-impact-engineering/special-issue/10MTGP5W4VJ
* Corresponding author. Tel.: +1-601-634-2039; fax: 1-601-634-2642.
E-mail address: Kent.T.Danielson@usace.army.mil.

Downloaded from http://asmedc.silverchair.com/hvis/proceedings-pdf/HVIS2019/883556/V001T02A009/6551025/v001t02a009-hvis2019-111.pdf by guest on 06 July 2022

and generally contain the more desirable hex elements in large regions of the mesh. In this paper, the four 2nd order element types depicted in Fig. 1 are used, which authors [4-6] have found to mass lump well for explicit methods and have well-defined contact

Fig. 1. 15-node tetrahedron, 19-node pyramid, 21-node wedge, and 27-node hexahedron type finite element topologies used in this paper; serendipity element versions are obtained by omitting the nodes on all faces and at the centroid

tractions that reliably perform well both with nearly incompressible materials and in flexural applications. Higher-order elements avoid many of the problems of 1st order ones, but at an increased computational cost per element. Second-order elements seem to be a "sweet spot" in terms of accuracy and computational cost for impact analyses. These 2nd order elements eliminate the need for hourglass control and provide higher resolution with fewer elements, since a single element can inherently capture curvature and flexural modes. Second order elements can also simplify meshing, since they are less prone to volumetric locking associated with near incompressibility, such as what occurs in metal plasticity, than certain types of 1st order elements. Methods to avoid severe locking at the element level permit unstructured meshing, e.g., typical all-tet methods or hexahedral-dominant methods. These technologies were developed within the in-house meshing (ProMesher), parallel analysis (*ParaAble*), and visualization (PenView) codes as well as placed into popular production software for meshing (Cubit), parallel analysis (EPIC), and visualization (ParaView). The IMPETUS AFEA [7] and LS-DYNA [8] explicit finite element codes have also implemented similar elements. As part of this paper, the authors will also present some initial promising findings of similar performances for the natural extension of these works to a 19-node 2nd order pyramid element, which can additionally facilitate meshing.

2. Finite element formulation

2.1. Discrete equations of motion

The basic form of the Lagrangian nonlinear equations is derived as that in standard texts, e.g., [9-12]. The motion is described by the current position of any point, at time, t, related to the undeformed position, $\mathbf{X}$, using the displacements, $\mathbf{u}$, from the undeformed configuration. The virtual work for large strain/deformation dynamic equilibrium at any time is defined with the body forces per unit mass, $\mathbf{b}$, e.g., gravity accelerations, the applied surface tractions, $\hat{\mathbf{t}}$, and the inertia forces all moving through virtual displacements, $\delta\mathbf{u}$, from the deformed configuration. It is spatially discretized into a mesh of standard displacement-based isoparametric Galerkin elements; their general formulations are found in the literature for many different element types, e.g., [9-12], and for those herein, in references [4-6]. In addition, an augmented version of the 13/14-node pyramid elements [13] to include all face and the body centroid nodes is used. Defining h as the shape function and q as a generalized degree of freedom, the general elemental equation for node, I, at time, t, is

$$\left[\int_{V_o} \boldsymbol{\rho_o \ddot{u} h_I} dV_o\right] \boldsymbol{\delta q_I} = \left[\int_{V_o} \boldsymbol{\rho_o b_q h_I} dV_o + \int_{A_d} \hat{\boldsymbol{t}}_q \ddot{\boldsymbol{u}} dA_d + \int_{V_o} \boldsymbol{\sigma} : \boldsymbol{\partial h_I / \partial x} \, dV_d\right] \boldsymbol{\delta q_I} \tag{1}$$

where δ is the variational operator designating a virtual quantity, the subscript d refers to the deformed configuration, each dot refers to differentiation with respect to time, ρ_d is the current mass density, and A_d and V_d are the deformed configuration surface area and volume, respectively. $\boldsymbol{\sigma}$ are Cauchy (true) stresses. The displacement boundary conditions are satisfied by explicitly controlling the motion of each appropriate nodal point by user model input at runtime. The acceleration, body force, and applied traction components with the q subscript are the values in the direction of the generalized degree of freedom. The virtual quantities are virtual nodal displacements that are now factored out, so that the elemental equation for each degree of freedom is defined by the expressions within the square brackets of Eq. (1). Large deformations are accommodated by the incremental transient explicit time integration procedures.

2.2. Numerical methods

Either "Full" (exact for ideal shape) quadrature rules are used for compressible materials or "Selective Reduced" (SR appended to the names in Fig. 1) integration for nearly incompressible materials to address volumetric locking [13, 14], whereby deviatoric and pressure terms use "Full" and a lower-order "Reduced" quadrature, respectively. Following [4-6], the higher-order elements considered herein use a row summation scheme for mass lumping, whereby all of the components in the row are summed and placed on the diagonal. A central difference scheme is used for temporal integration, e.g., [8, 15-19] without mass scaling, damping, or other special procedures. A simple 1-D wave propagation approach approximates a critical time increment, using a

Downloaded from http://asmedc.silverchair.com/hvis/proceedings-pdf/HVIS2019/883556/V001T02A009/6551025/v001t02a009-hvis2019-111.pdf by guest on 06 July 2022

shortest distance between pairs of adjacent nodes in each element and fastest material sound wave speed of the corresponding element to compute the time required to transverse that distance. Artificial viscosity (pressure) is added to the pressure in explicit methods [8, 15-19] to prevent element collapse in the presence of high-velocity gradients and to quiet truncation frequency oscillations or "ringing".

3. Examples

3.1. Cylindrical bar impact

Here, a cylindrical bar impacting a rigid frictionless wall at 227 m/s is modeled with a quarter symmetric mesh and definition similar to that in [3, 9]. The bar is 3.24×10^{-2} m long with a 3.2×10^{-3} m radius. The copper isotropic hardening plasticity model uses a modulus of elasticity of 1.17×10^{11} Pa, Poisson's ratio of 0.33, yield stress of 4.00×10^{8} Pa, tangent plastic modulus of 1.00×10^{8} Pa, and mass density of 8930 kg/m^3. Figure 2 shows undeformed and deformed plots of the hexahedral-dominant model using TET15SR, PYR19SR, and WEG21SR elements placed along the bar centerline at the impact zone and HEX27SR elements placed elsewhere. The model predictions of 7.3612451 mm and 21.465609 mm for the final radius and length, respectively, compare favorably with the results in [3, 9].

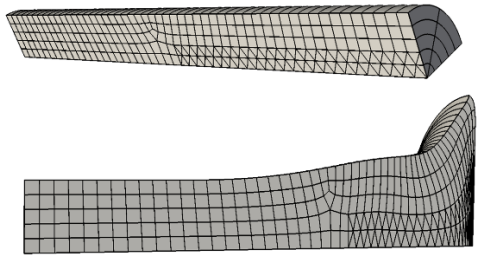

Fig. 2. Deformed unstructured mesh plots for bar impact problem using Quarter-symmetry 2nd Order Hex-Dominant mesh of HEX27SR, WEG21SR, PYR19SR, and TET15SR type elements.

3.2. Penetration into concrete using cavity expansion functions

This example models the penetration of a solid ogive-nose projectile into a concrete half-space using cavity expansion penetration resistance functions, as in [20] with penetration test data [21]. The projectile has a 3.0 CRH ogive-nose, shank length of 169.5 mm, nose length of 33.7 mm, and shank diameter of 20.3 mm. It is made of 4340 R_c 45 steel and modeled with a power law hardening elastic-plastic model with modulus of elasticity of 206.8 GPa, Poisson Ratio of 0.32, yield stress of 1.207 GPa, hardening constant of 382 MPa, hardening exponent of 0.266, plastic modulus of 141 MPa, and mass density of 7810 kg/m^3. The concrete has an unconfined strength of 58.4 MPa, mass density of 2320 kg/m^3, and a cavity expansion S-factor of 9.037.

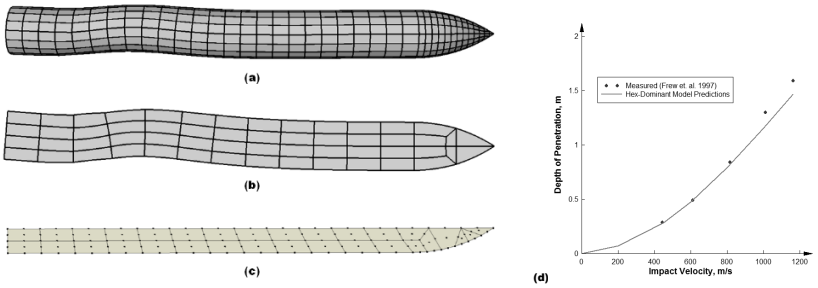

Fig. 3. Model plots for (a) Full-symmetry deformed 1st order brick mesh [33]; (b) Half-symmetry deformed 2nd Order Hex-Dominant mesh; (c) Undeformed Half-symmetry 2nd Order 2-D mesh Automatically created by a Paving Algorithm; and (d) test and predicted results for normal impact.

Downloaded from http://asmedc.silverchair.com/hvis/proceedings-pdf/HVIS2019/883556/V001T02A009/6551025/v001t02a009-hvis2019-111.pdf by guest on 06 July 2022

Figure 3 shows (a) the 1st order model of [21]; (b) a 2nd order Hex-Dominant model requiring only a little user intervention; and (c) a 2nd order 2-D mesh automatically generated by a paving approach on the half cross-section. The three-dimensional model in Fig. 3(b) was created by simply revolving a user-created 2nd order 2-D mesh about the projectile axis to create a model of HEX27SR, WEG21SR, and TET15SR elements. The 2-D mesh in Fig. 3(c) was created automatically from the CAD geometry, which is especially beneficial for large tradespace or shape optimization applications that need to create numerous meshes. The automation, however, places elements with a single node on the axis of revolution. These are easily and automatically identified and accommodated in a 3-D mesher by splitting the quadrilaterals into two triangles, and any triangle with a single node on the axis can now be automatically generated into a series of PYR19 elements by the rotation of the 2-D mesh. As seen in Fig. 3, the Hex-Dominant model predictions are in good agreement with the normal impact predictions and test data of the examples in [20-21], as well as with the 1st order hexahedron model for a non-normal impact velocity of 500 m/s with an Angle of Attack (AOA) of 5.0 degrees. For non-normal impact, the projectile models both predict very similar final positions at about a 0.27 m depth and a double permanent bending in the aft end. The 1st order model used default hourglass control parameters and the 2nd order model, of course, represents hourglass modes naturally without resorting to methods of artificial control.

4. Concluding remarks

The results show that the 2nd order elements have distinct advantages for certain applications, especially for flexure, curved geometries, and unstructured meshes with nearly incompressible materials, and are thus useful for 2nd order Hex-Dominant approaches that can greatly simplify and automate meshing. The ability to use unstructured combinations of the different element types in explicit dynamics codes provides an important modeling alternative to all-Hex or all-Tet meshing. The Hex-Dominant meshes are typically more computationally intensive than corresponding all-Hex models, but typically much less so than corresponding all-Tet models. The ability to automate meshing of reasonable sizes can significantly reduce analysts effort and is quite beneficial for applications like shape optimization.

Acknowledgements

Permission to publish was granted by Director, Geotechnical and Structures Laboratory.

References

[1] Meshkat S., Talmor D., 2000. Generating a mixed mesh of hexahedra, pentahedra and tetrahedra from an underlying tetrahedral mesh. Int J Numer Meth Eng 49:17–30
[2] Owen S., Saigal S., 2000. H-Morph: an indirect approach to advancing front hex meshing. Int J Numer Meth Eng **49**:289–312
[3] Abaqus, 2018. CAE, Theory, Benchmarks, and Examples Manuals. Dassault Systèmes Simulia Corp., Providence, RI, USA
[4] Danielson K., Adley M., Williams T., 2016. Second-order finite elements for Hex-Dominant explicit methods in nonlinear solid dynamics. Finite Elements Anal Des 19:63–77.
[5] Danielson K., O'Daniel J., 2011. Reliable second-order hexahedral elements for explicit methods in nonlinear solid dynamics. Int J Numer Meth Eng 85(9):1073–1102. doi: 10.1002/nme.3003
[6] Danielson, K., 2014. Fifteen Node Tetrahedral Elements for Explicit Methods in Nonlinear Solid Dynamics. Comput Meth Appl Mech Eng 272:160-180, ISSN 0045-7825, http://dx.doi.org/10.1016/j.cma.2014.01.012
[7] IMPETUS AFEA, 2012. SOLVER, User Documentation, version 3.0 beta, IMPETUS AFEA, Flekkefjord, Norway
[8] LS-DYNA, 2012. KEYWORD USER'S MANUAL VOLUME I, Version 971 R6.1.0. Livermore Software Technology Corporation, Livermore, CA
[9] Zienkiewicz O., Taylor R., Zhu J., 2005. The finite element method: its basis and fundamentals; The finite element method for solid and structural mechanics, sixth edition. Elsevier Butterworth-Heinemann, Burlington, MA
[10] Bathe K-J., 1996. Finite Element Procedures. Prentice-Hall, Englewood Cliffs, New Jersey
[11] Belytschko, T., Liu, W., Moran, B., 2000. Nonlinear Finite Elements for Continua and Structures. John Wiley & Sons, New York
[12] Hughes T. 1987. The finite element method linear static and dynamic finite element analysis. Prentice-Hall, Englewood Cliffs, NJ
[13] Felippa, C., 2004. "A compendium of FEM integration formulas for symbolic work", Engineering Computations, Vol. 21 Issue: 8, pp.867-890, https://doi.org/10.1108/02644400410554362
[14] Nagtegaal J., Parks D., Rice J., 1977. On numerically accurate finite element solutions in the fully plastic range. Comput Meth Appl Mech Eng 4:153-177
[15] Presto User's Guide Version 4.16 ., 2012. Report SAND2010-3112, Sandia National Laboratories, Albuquerque, NM
[16] Zywicz E., Lin J., 2012. DYNA3D: A nonlinear, explicit, three-dimensional finite element code for solid and structural mechanics: version 12.1. Lawrence Livermore National Laboratory Report, LLNL-SM-599533. Livermore, CA
[17] Benson D., 1992. Computational methods in Lagrangian and Eulerian hydrocodes. Comput Meth Appl Mech Eng 99:235-394
[18] Taylor L., Flanagan D., 1989. PRONTO 3D: A three-dimensional transient solid dynamics program. Report SAND 87-1912, Sandia National Laboratories, Albuquerque, NM

Downloaded from http://asmedc.silverchair.com/hvis/proceedings-pdf/HVIS2019/883556/V001T02A009/6551025/v001t02a009-hvis2019-111.pdf by guest on 06 July 2022

[19] Johnson G., Beissel S., Gerlach C., Holmquist T., Stryk R., 2010. User Instructions for the 2010 Version of the EPIC Code, Southwest Research Institute, Final Report, Contract W56HZV-06-C-0194 with U.S. Army RDECOM-TARDEC.
[20] Warren T., Tabbara M., 1997. Spherical cavity-expansion forcing function in PRONTO 3D for applications to penetration problems. SAND97-1174, Sandia National Laboratories, Albuquerque, NM.
[21] Frew, D., Hanchak, S., Green, M., Forrestal, M., 1998. Penetration of concrete targets with ogive-nose steel rods. Int J Impact Engng 21(6):489-497

Downloaded from http://asmedc.silverchair.com/hvis/proceedings-pdf/HVIS2019/883556/V001T02A009/6551025/v001t02a009-hvis2019-111.pdf by guest on 06 July 2022

This material is declared a work of the U.S. Government and is not subject to copyright protection in the United States.
Approved for public release; distribution is unlimited.